Nanomaterials

DOI: 10.1002/anie.200705111

Direct Light-Driven Modulation of Luminescence from Mn-Doped ZnSe Quantum Dots**

*Scott E. Irvine, Thorsten Staudt, Eva Rittweger, Johann Engelhardt, and Stefan W. Hell**

Quantum dot (QD) nanocrystals remain at the forefront of fluorescence microscopy as they have the advantages of enhanced photostability, high quantum yield, and macromolecular size.[1–3] Furthermore, the ability to tune the QD fluorescence, either by changing their size[1] or by doping,[4] allows for multiplexed imaging. The range of applications extends well beyond the realm of microscopy: QDs may also play a major role in developing novel photonic devices including lasers, light-emitting diodes, and displays.[5–7]

Despite significant advancements in nanocrystal research, the inability to directly modulate the fluorescence from QDs has precluded their implementation in several areas. In particular, emerging far-field diffraction-unlimited microscopy techniques[8] uniquely benefit from the capability to reversibly modulate/switch fluorescent ensembles from a bright "on" state to a dark "off" state. This activation must occur as a response to optical stimuli which do not contain spectral components within the excitation kernel of the fluorescent markers. With the need for optical control over QD fluorescence, indirect methods have been conceived by using hybrid QD structures[9–11] that incorporate a photochromic activator/quencher. Although the concept has been clearly established, hybrid QD structures suffer from inherent drawbacks, such as inadequate photostability, limited fluorescence quenching, and sensitivity to local environment/solvent.

Herein we report on the direct light-driven modulation of QD fluorescence. The mechanism for the fluorescence modulation relies only on internal electronic transitions within Mn-doped ZnSe quantum dots (Mn-QDs). It is demonstrated that the fluorescence of the QD can be reversibly depleted with efficiencies of over 90% by using continuous-wave optical intensities of approximately 1.9 MW cm^{-2}. Time-domain measurements during the modulation indicate that the number of fluorescent on–off cycles exceeds 10^3 before a significant reduction in the fluorescence quantum efficiency occurs. Such robust nanometric probes having remotely controllable optical transitions are useful in many areas of research, particularly in far-field nanoscopy based on reversible saturable or switchable optical fluorescence transitions (RESOLFT).[8] Consequently, we show that implementation of Mn-QDs for imaging leads to an increase in the resolution by a factor of 4.4 over that of confocal microscopy.

A schematic diagram of the electronic transitions involved in light-modulated fluorescence from Mn-QDs is shown in Figure 1a. Initially, electrons are photoexcited from the valence band to the conduction band of the ZnSe semiconductor host. Within a short time (picosecond timescale[12–14]), the excited electrons are transferred to the $^4T_1$ upper florescent state of the Mn^{2+} ion and decay radiatively to the $^6A_1$ state within a measured fluorescence lifetime of $\tau_{fluo} \approx 90$ μs (see the Supporting Information). Generally speaking, direct modulation of the fluorescence requires active control over a process that competes with spontaneous emission. In the case of doped semiconductors and glasses, excited-state absorption (ESA) can occur from the upper

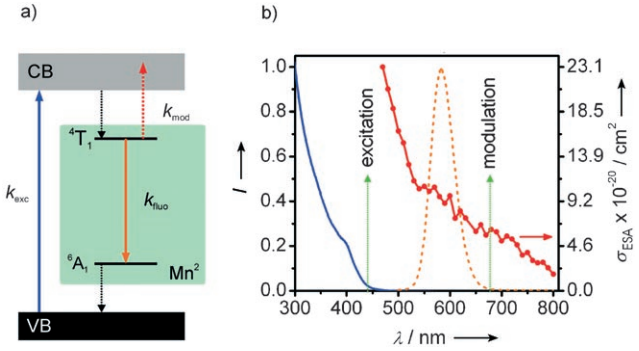

Figure 1. a) Schematic diagram of the electronic transitions involved in modulating fluorescence from Mn-QDs. Initially, electrons are pumped (k_{exc}) from the valence band (VB) to the conduction band (CB) of the ZnSe host, and are subsequently transferred to the $^4T_1$ level of the Mn^{2+} dopant. Here, the electrons can relax radiatively (k_{fluo}) to the $^6A_1$ level; however, they can also be pumped (k_{mod}) to higher levels through excited-state absorption (ESA) from the $^4T_1$ state. b) Absorption (solid blue line), emission (dotted orange line), and ESA spectra (red line and circles, right vertical scale) of the Mn-QDs. The locations of the excitation and modulation wavelengths in the spectra are also indicated with green vertical arrows.

[*] Dr. S. E. Irvine, T. Staudt, E. Rittweger, Prof. Dr. S. W. Hell
Department of Nanobiophotonics
Max Planck Institute for Biophysical Chemistry
Am Fassberg 11, 37077 Göttingen (Germany)
Fax: (+49) 551-201-2505
E-mail: shell@gwdg.de

T. Staudt, Dr. J. Engelhardt, Prof. Dr. S. W. Hell
German Cancer Research Center
High Resolution Optical Microscopy Division
Bioquant-Zentrum, Im Neuenheimer Feld 267,
69120 Heidelberg (Germany)

[**] S.E.I. and T.S. contributed equally to this work. This work was supported by the European Union through the SPOTLITE project (New and Emerging Science and Technology). S.E.I. also gratefully acknowledges support from the Natural Sciences and Engineering Research Council of Canada (NSERC).

Supporting information for this article is available on the WWW under http://www.angewandte.org or from the author.

fluorescent level of the impurity ion to higher lying states within either the dopant or the conduction band of the host material. Depending on the specific density of states above $^4T_1$, red-shifted light (with respect to the excitation) can be used to invoke the ESA mechanism to selectively pump electrons out of the $^4T_1$ state and inhibit spontaneous fluorescence emission, while avoiding further excitation from the ZnSe host.

The room-temperature absorption and photoluminescent spectra of the Mn-QDs are shown in Figure 1b. Absorption from the ZnSe host is clearly observed, with the first exciton band occurring at a wavelength of about 400 nm. Fluorescent emission is centered at a wavelength of 580 nm with a full-width at half-maximum value of approximately 50 nm, which is a hallmark of the $^4T_1 \rightarrow {}^6A_1$ transition of the Mn^{2+} dopant.[4] Measurement of the ESA spectrum of the Mn-QDs was carried out using an experimental arrangement described elsewhere.[15] Briefly, absorption from the excited state was quantified by phase-sensitive lock-in measurements, in which a white-light probe passing through a solution of the Mn-QDs experienced a spectrally-dependent transient absorption that was directly correlated with the chopped excitation beam. The results of this measurement are shown in Figure 1b, where it is observed that the ESA spectrum spans a large portion of the visible window. Similar results have also been obtained for bulk Mn-doped ZnSe[16] and Co-doped ZnSe.[17] Other glasses doped with rare-earth elements[18] also show broadband impurity–host transitions that exhibit a large dependence on the particular host material. Thus, an intensity-dependent loss channel that competes directly with the fluorescent emission can be introduced to efficiently modulate the luminescence originating from the $^4T_1 \rightarrow {}^6A_1$ transition.

Experimentally, the spectroscopic criteria for fluorescence imaging of the Mn-QDs are fulfilled using collinear laser sources at $\lambda_{exc} = 440$ nm and $\lambda_{mod} = 676$ nm for excitation and modulation, respectively. Radiation from the two sources is coupled into a scanning confocal microscope, and their corresponding intensities I_{exc} and I_{mod} are controlled by using acoustooptic tunable filters. The extended lifetime (ca. 90 μs) of the $^4T_1 \rightarrow {}^6A_1$ transition of the Mn^{2+} ion limits the number of excitation–emission sequences a single Mn-QD can perform within a given time frame. Thus, the fluorescent photon emission rate is lifetime-limited, thereby challenging optical imaging of single isolated Mn-QDs. As an alternative, multi-QD ensembles were prepared on a glass coverslip to reach adequate fluorescence intensity levels (I_{fluo}). Atomic force microscopy studies on the Mn-QD ensembles indicate a large distribution of sizes that range from 20 to 300 nm.

Confocal images of the ensembles are shown in Figure 2a for $I_{exc} = 50\ W\,cm^{-2}$ and $I_{mod} = 9\ MW\,cm^{-2}$. Here, I_{mod} was toggled with every tenth scan step along the x axis, which resulted in dark lines along the vertical direction where the fluorescence was selectively inhibited. This emphasizes the degree of optical control over the QD luminescence as well as its reversible nature. Measurement of the degree of fluorescence inhibition was carried out through acquisition of several of confocal images of Mn-QDs for various values of I_{mod}. Results of this experiment are illustrated in Figure 2b in

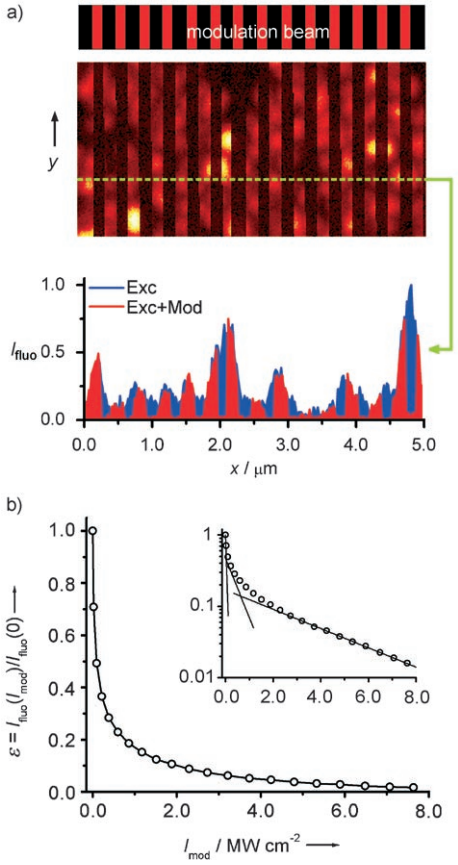

Figure 2. a) Confocal images of Mn-QD ensembles. Dark lines along the y direction demonstrate the capability to actively and reversibly control fluorescence emitted from solid-state nanocrystals. Intensities of $I_{exc} = 50\ W\,cm^{-2}$ and $I_{mod} = 9\ MW\,cm^{-2}$ were utilized. A line section through the confocal image shows the fluorescence response and the high efficiency of modulation (red) overlaid with a similar line cut (blue) through the corresponding image having $I_{mod} = 0$ (not shown). b) Depletion curve indicating the normalized residual fluorescence ε as a function of modulation intensity I_{mod}. At $I_{mod} = 1.9\ MW\,cm^{-2}$, the fluorescence level is reduced to 10% of its original value. The logarithmic representation (inset) indicates a multiexponential fluorescence depletion process. A triple exponential has been fitted to the data and has characteristic decay constants of 0.043, 0.52, and 3.22 $MW\,cm^{-2}$, each of which have been illustrated by a solid line.

terms of the residual fluorescence $\varepsilon = I_{fluo}(I_{mod})/I_{fluo}(0)$ as a function of I_{mod}. The effectiveness of the fluorescence inhibition process is clear, as $\varepsilon < 10\%$ can be achieved for $I_{mod} = 1.9\ MW\,cm^{-2}$. The inset of Figure 2b contains a logarithmic plot of the fluorescence depletion and reveals the existence of multiple depletion channels, which is consistent with the large density of states above $^4T_1$ provided by the ZnSe conduction band as well as the upper manifold of the Mn^{2+} impurity.[19,20]

Depending on the nonradiative decay across the ZnSe bandgap, it is possible that electrons which are momentarily shelved above the $^4T_1$ state by I_{mod} are allowed to cycle between the conduction band of the host and the $^4T_1$ fluorescent state of the Mn^{2+} dopant. The degree of cycling can be readily ascertained by comparing the ESA cross-section (σ_{ESA}) determined directly from transient absorption

measurements (Figure 1b) with the net ESA cross-section calculated from the fluorescence depletion curve (Figure 2b). The net cross-section for ESA (ζ_{ESA}) for raising electrons from the $^4T_1$ state to the conduction band of the ZnSe host can be determined from the competition between the fluorescence decay rate k_{fluo} and ESA-induced pump rate k_{mod}. Given that $k_{mod} = \zeta_{ESA} I_{mod}$ and $k_{fluo} = 1/\tau_{fluo}$, the value of ζ_{ESA} can be calculated from the fact that the condition $k_{mod} = k_{fluo}$ is satisfied at $\varepsilon = 50\,\%$. Thus, a value of $\zeta_{ESA} = 2.1 \times 10^{-20}$ cm^2 is estimated, which compares well with the value of $\sigma_{ESA} = 6.1 \times 10^{-20}$ cm^2 (at 676 nm) shown in Figure 1b and those determined previously for other Mn^{2+} ion/host systems.[19] The fact that ζ_{ESA} and σ_{ESA} have the same order of magnitude indicates that a significant amount of electronic cycling does not occur. Furthermore, no up-converted emission from the terminal states of the ESA transition could be detected in the spectral region between 420 and 1100 nm. Based on this evidence, it is concluded that nonradiative transitions dominate electron relaxation to the valence band during fluorescence depletion.

To ascertain the modulation photostability of Mn-QDs, the excitation and modulation beams were focused on an isolated ensemble, without scanning, and the modulation beam was interrupted at a frequency of 25 Hz. The resultant time-domain fluorescence signal is shown in Figure 3, which

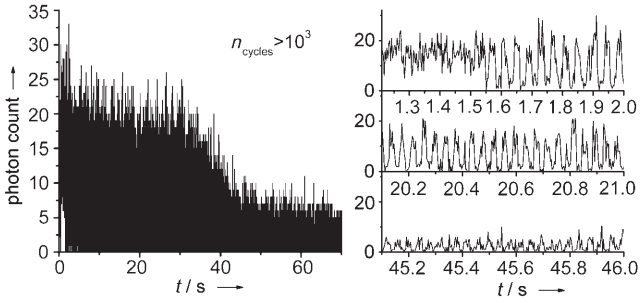

Figure 3. Temporal fluorescent response from a Mn-QD ensemble under conditions of steady-state excitation at 100 W cm^{-2} and transient depletion at $I_{mod} = 1.9$ MW cm^{-2}, in which I_{mod} is interrupted at a frequency of 25 Hz. Fluorescent modulation persists for nearly 40 seconds (ca. 10^3 cycles) before the cluster photobleaches significantly. Several smaller panels illustrate the digital-like switching over time-scales comparable to the modulation period.

provides clear evidence of the robustness of the ESA-mediated fluorescence-inhibition process. Continuous excitation and depletion of the fluorescence persists for nearly 40 seconds before the quantum efficiency degrades substantially as a result of photobleaching. Within this measurement time frame, the single Mn-QD cluster undergoes on average 10^3 fluorescence modulation cycles.

Efficient switching and stable on–off modulation are highly desirable attributes for advanced microscopy techniques. A primary example for which the Mn-QDs are suited is RESOLFT imaging,[21] which relies on reversibly photoswitchable luminescent compounds to achieve optical resolutions below the diffraction limit.[22] This resolution is here realized in a two-beam scanning confocal arrangement: one laser source was used to excite the photomarkers, while another spatially overlapped beam featuring an intensity null[23] selectively inhibited fluorescence everywhere except regions near the null. In this particular case, the resulting intensity distribution features a zero line in the focal plane, where the fluorescence is effectively "squeezed" along one axis that is perpendicular to the zero line (see the Supporting Information).

A reference confocal image of clusters of Mn-QDs is shown in Figure 4b. Several isolated clusters are present and exhibit diffraction-limited full-width at half maximum values

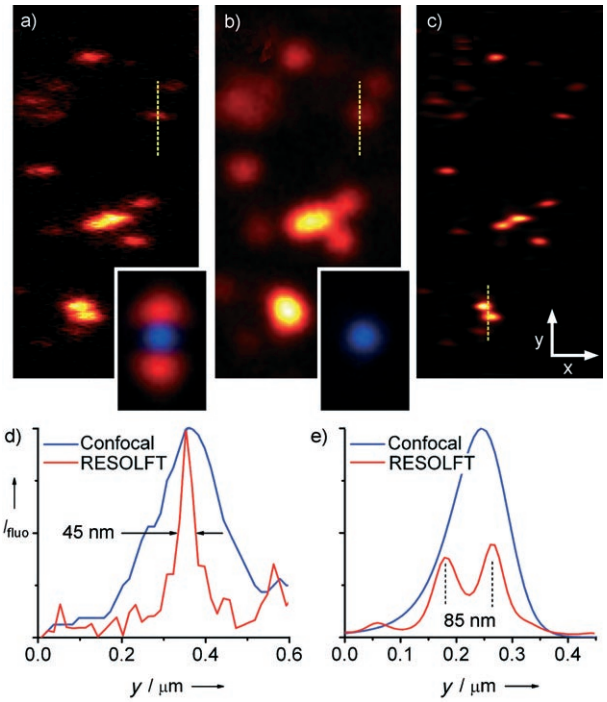

Figure 4. Image acquired using the RESOLFT technique (a), which has a clear improvement in resolution along the *y* direction in comparison to the purely confocal counterpart (b). The insets illustrate the effective PSFs of the excitation and modulation beams: a) excitation overlapped with the inhibition beam and b) only excitation. Richardson–Lucy deconvolution was applied to (a) and the result is shown (c). For comparison, a one-dimensional line section (indicated by a yellow dashed line) through a representative RESOLFT PSF (a) and its diffraction-limited counterpart (b) are plotted separately in panel (d). The enhanced resolution is clear, as the 200-nm diffraction-limited PSF is effectively reduced to 45 nm. A similar section from (c) as well as its corresponding deconvoluted confocal counterpart (not shown) are illustrated in (e), which reveals that structures separated by 85 nm can be distinguished using RESOLFT, which otherwise appear as a single peak in the confocal reference spectrum.

of 200 nm. Larger features are also present, as indicated by their relative brightness, although no information can be obtained regarding the substructure. RESOLFT images of the same region are shown in Figure 4a. Whereas single isolated clusters appear as nearly spherically symmetric intensity distributions in the confocal image, the corresponding point-spread functions (PSFs) in the RESOLFT image have been substantially reduced along the *y* axis by the spatially structured modulation beam.

A cross-section through a representative PSF is shown in Figure 4d, which has a full-width at half-maximum value of 45 nm; a factor of 4.4 improvement over the corresponding confocal PSFs and nearly a factor of 10 smaller than the λ_{exc} value. The size of the PSFs can be compared with the theoretical resolution determined by Equation (1):[8]

$$\Delta r = \frac{\lambda}{2n\sin(\alpha)\sqrt{1+I_{max}/I_s}} \quad (1)$$

where n is the index, α is the aperture angle of the objective, and λ and I_{max} are the wavelength and maximum intensity of the modulation beam, respectively. Here I_s is defined as the depletion intensity required to reduce the fluorescence to one half of the original value, which is determined from Figure 2b to be $I_s = 0.1\ MW\,cm^{-2}$. Given a local intensity of $I_{max} = 2.5\ MW\,cm^{-2}$, as well as $n = 1.5$ and $\alpha = 60°$, the value of Δr can be calculated to be 51 nm, which compares well with the measured value of 45 nm. Nonlinear deconvolution of the RESOLFT image results in the data shown in Figure 4c, where clear subdiffraction structure becomes apparent. Resolving such features was only possible after significantly expanding the optical transfer function of the microscope by optical modulation. Clear evidence of this is also shown in Figure 4e. Two clusters separated by 85 nm can be clearly distinguished in the RESOLFT image, but appear as a single peak within the corresponding confocal scan.

In conclusion we have demonstrated the reversible and wavelength-selective optical modulation of fluorescence from Mn^{2+}-doped ZnSe quantum dots. This process relies on excited-state absorption and its direct control of quantum dot fluorescence by light. Experiments demonstrate that all optical-switching efficiencies above 90% can be achieved using continuous-wave laser sources operating near 1 mW. The ability to invoke the fluorescence modulation using continuous-wave radiation, as well the advanced on–off photostability afforded by quantum nanocrystals, opens new avenues of research and application of optically activated quantum dots. As a primary example, Mn-QDs can be implemented for nanoscale imaging. This highlights the relevance of these photoswitchable QDs to contemporary nanoscopy as well as to other future applications, such as biological assays that require the stability afforded of quantum dots and the direct control of their fluorescence capability by light. Last but not least, we have described yet another optical microscopy modality that exploits bright and dark states of a (fluorescent) marker to break the diffraction barrier,[8,22] thus underscoring the general nature of this strategy.

Experimental Section

Quasicontinuous excitation of the Mn-doped quantum dots (NN-Labs, Fayetteville, AR) was achieved using a high-repetition rate laser diode source (PicoQuant, Berlin, Germany) at a wavelength of $\lambda_{exe} =$ 440 nm, which had an interpulse dwell time (200 ns) much shorter than the lifetime of the Mn-doped quantum dots (ca. 90 us). Fluorescence depletion at $\lambda_{mod} = 676$ nm was accomplished using a continuous-wave Ar-Kr laser (Spectra Physics-Division of Newport Corporation, Irvine, CA). The excitation and modulation beams were combined using acoustooptic tunable filters (Crystal Technologies, Palo Alto, CA) and coupled into a stage-scanning confocal microscope. Collected fluorescence passed through an additional band-pass filter (40 nm band-pass centered at 580 nm, AHF Analysentechnik, Tübingen, Germany) and was detected with a photon-counting module (SPCM-AQR-13-FC, PerkinElmer, Canada). Two identical adjacent optical flats were used to provide a 180° phase discontinuity midway through the modulating beam to generate a beam profile containing a zero-line for RESOLFT experiments.

Received: November 5, 2007
Published online: February 27, 2008

Keywords: fluorescence · nanostructures · photochemistry · photophysics · quantum dots

[1] X. Michalet, F. F. Pinaud, L. A. Bentolila, J. M. Tsay, S. Doose, J. J. Li, G. Sundaresan, A. M. Wu, S. S. Gambhir, S. Weiss, *Science* **2005**, *307*, 538.
[2] A. Sukhanova, M. Devy, L. Venteo, H. Kaplan, M. Artemyev, V. Oleinikov, D. Klinov, M. Pluot, J. H. M. Cohen, I. Nabiev, *Anal. Biochem.* **2004**, *324*, 60.
[3] P. Reiss, J. Bleuse, A. Pron, *Nano Lett.* **2002**, *2*, 781.
[4] N. Pradhan, D. M. Battaglia, Y. C. Liu, X. G. Peng, *Nano Lett.* **2007**, *7*, 312.
[5] V. I. Klimov, S. A. Ivanov, J. Nanda, M. Achermann, I. Bezel, J. A. McGuire, A. Piryatinski, *Nature* **2007**, *447*, 441.
[6] H. Mattoussi, L. H. Radzilowski, B. O. Dabbousi, E. L. Thomas, M. G. Bawendi, M. F. Rubner, *J. Appl. Phys.* **1998**, *83*, 7965.
[7] H. Song, S. Lee, *Nanotechnology* **2007**, *18*.
[8] S. W. Hell, *Science* **2007**, *316*, 1153.
[9] L. Y. Zhu, M. Q. Zhu, J. K. Hurst, A. D. Q. Li, *J. Am. Chem. Soc.* **2005**, *127*, 8968.
[10] E. Jares-Erijman, L. Giordano, C. Spagnuolo, K. Lidke, T. M. Jovin, *Mol. Cryst. Liq. Cryst.* **2005**, *430*, 257.
[11] I. L. Medintz, S. A. Trammell, H. Mattoussi, J. M. Mauro, *J. Am. Chem. Soc.* **2004**, *126*, 30.
[12] Y. Hefetz, W. C. Goltsos, A. V. Nurmikko, L. A. Kolodziejski, R. L. Gunshor, *Appl. Phys. Lett.* **1986**, *48*, 372.
[13] R. N. Bhargava, D. Gallagher, X. Hong, A. Nurmikko, *Phys. Rev. Lett.* **1994**, *72*, 416.
[14] T. Kuroda, H. Ito, F. Minami, H. Akinaga, *J. Lumin.* **1997**, *72–4*, 106.
[15] E. Rittweger, B. R. Rankin, V. Westphal, S. W. Hell, *Chem. Phys. Lett.* **2007**, *442*, 483.
[16] J. Dreyhsig, U. Stutenbaumer, H. E. Gumlich, J. W. Allen, *J. Cryst. Growth* **1990**, *101*, 443.
[17] A. Ehlert, J. Dreyshig, H. E. Gumlich, J. W. Allen, *J. Lumin.* **1994**, *60–1*, 21.
[18] J. K. Lawson, S. A. Payne, *Phys. Rev. B* **1993**, *47*, 14003.
[19] R. Clausen, K. Petermann, *IEEE J. Quantum Electron.* **1988**, *24*, 1114.
[20] K. Petermann, R. Clausen, E. Heumann, M. Ledig, *Opt. Commun.* **1989**, *70*, 483.
[21] S. W. Hell, M. Dyba, S. Jakobs, *Curr. Opin. Neurobiol.* **2004**, *14*, 599.
[22] V. Westphal, S. W. Hell, *Phys. Rev. Lett.* **2005**, *94*, 143903.
[23] J. Keller, A. Schönle, S. W. Hell, *Opt. Express* **2007**, *15*, 3361.

